Electrochemical Society Proceedings Vol. 2002-4, 139-149 (2002)

HIGH-EFFICIENCY MQW ELECTROABSORPTION MODULATORS

J. Piprek, Y.-J. Chiu, S.-Z. Zhang[(1)], J. E. Bowers,

C. Prott[(2)], and H. Hillmer[(2)]

University of California, ECE Department, Santa Barbara, CA 93106

[(1)] now with Zaffire, Inc., San Jose, CA 95134

[(2)] Universität GH Kassel, Technische Elektronik,

34132 Kassel, Germany

ABSTRACT

Multi-quantum well (MQW) electroabsorption modulators (EAMs) are attractive for applications requiring signal modulation at high speed and with high efficiency (high extinction ratio at low voltage). They are promising devices for external signal modulation in high-bandwidth optical communication systems. EAMs can be integrated with other devices like laser diodes, semiconductor optical amplifiers, and mode transformers. We have fabricated InGaAsP/InP multi-quantum well EAMs with a bandwidth above 25 GHz and with up to 35dB/V extinction efficiency. We analyze the transmission performance of our modulator in detail and identify optimum operation conditions.

1. INTRODUCTION

Electroabsorption modulators are attractive for applications requiring high speed modulation, low drive voltage, high extinction ratio, and integrability. They are promising devices for external signal modulation in high-bandwidth optical communication systems. EAMs can be integrated with other devices like laser diodes, semiconductor optical amplifiers, and mode transformers. EAMs are based on the electroabsorption effect, i.e., on the change of the absorption coefficient due to an electric field. In bulk semiconductors, the absorption edge moves to lower energies with increasing electric field due to a combination of band-to-band absorption and tunneling processes (Franz-Keldysh effect).

In quantum wells, the transition energy between confined energy levels for electrons and holes is reduced as an electric field is applied in growth direction (quantum confined Stark effect, QCSE). This effect is illustrated in Fig. 1. As the field is increased, the overlap of electron and hole wavefunctions is reduced thereby decreasing the absorption strength at the transition energy. Thick quantum wells are advantageous for high field sensitivity (high modulation efficiency) whereas thin quantum wells give stronger absorption. The formation of electron-hole pairs (excitons) in the quantum well enhances the absorption.[1] Theoretical absorption spectra are shown

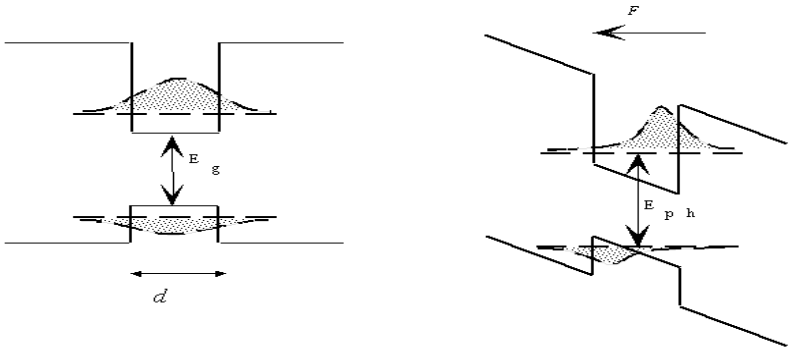

Figure 1. Quantum well band edges, quantum levels, and electron wave functions with (right) and without (left) applied electric field F (E_g - bulk band gap, E_{ph} - transition energy).

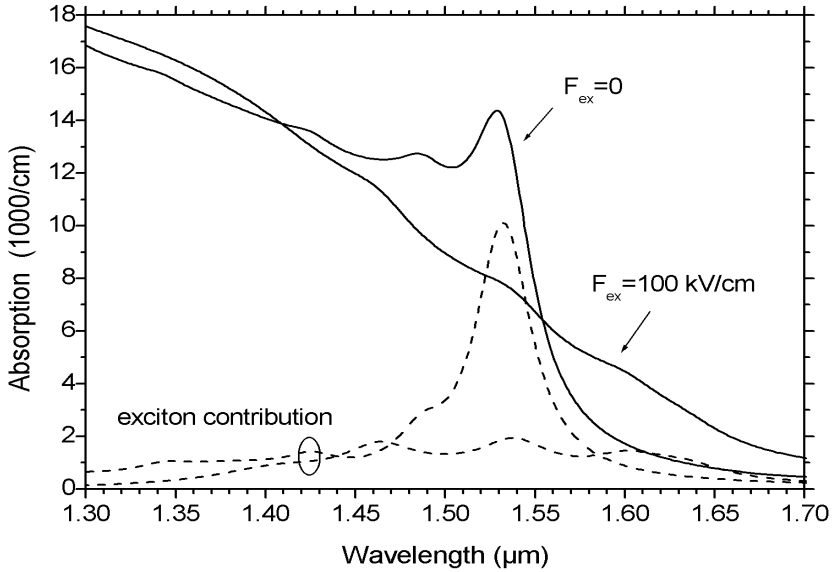

Figure 2. Absorption spectra calculated at two different electric fields. The dashed lines give the exciton contribution to the total absorption (solid).

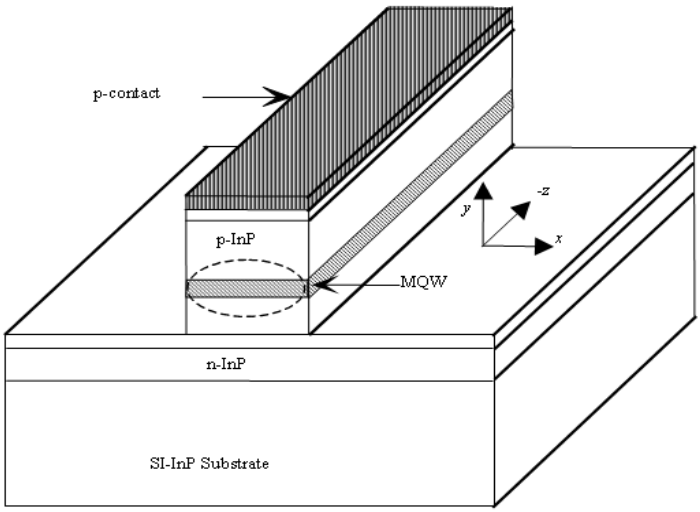

Figure 3. Schematic device structure with the optical mode indicated by the dashed line (ridge width W = 2μm, length L = 300μm).

in Fig. 2 as computed for our quantum wells using the model in Ref..[2] Parabolic bands are assumed in this calculation. Contributions by excitons, confined quantum well states, and extended states are included. The total absorption is shown at two different electric fields (solid lines). With higher field, the absorption edge moves to longer wavelengths, as expected. In addition, the slope of the absorption edge is reduced due to the vanishing exciton contribution (dashed lines). At and above room temperature, the ionization of excitons is typical at high electric fields, however, it reduces the EAM efficiency.

2. DEVICE STRUCTURE AND EXPERIMENTAL RESULTS

The schematic device design is given in Fig. 3. The 300μm long ridge waveguide structure is grown by MOCVD on semi-insulating InP. The ridge structure consists of a 0.3 μm n-InP cladding layer, 10 strain-compensated InGaAsP quantum wells (10.4 nm wide, 0.37% tensile strain), 11 InGaAsP barriers (7.6 nm wide , 0.5% compressive strain), a 1.5 μm p-InP cladding layer and a 0.1 μm p-InGaAs top contact layer. The ridge is 2μm wide and etched through the MQW region. The etch-stop layer is also used as n-contact layer. PMGI is used to passivate the sidewalls and to reduce the capacitance due to the p-electrode on the optical waveguide. The energy band diagram of our active region is plotted in Fig. 4 at zero bias, indicating a significant build-in electrostatic field. Including the undoped InP regions, the total intrinsic (i) region thickness of our *pin* structure is about 300 nm. A fabricated InGaAsP/InP MQW EAM is shown in Fig. 5. Coplanar waveguide (CPW) electrodes are designed for both the microwave feed line region and the optical waveguide region (Fig. 6).

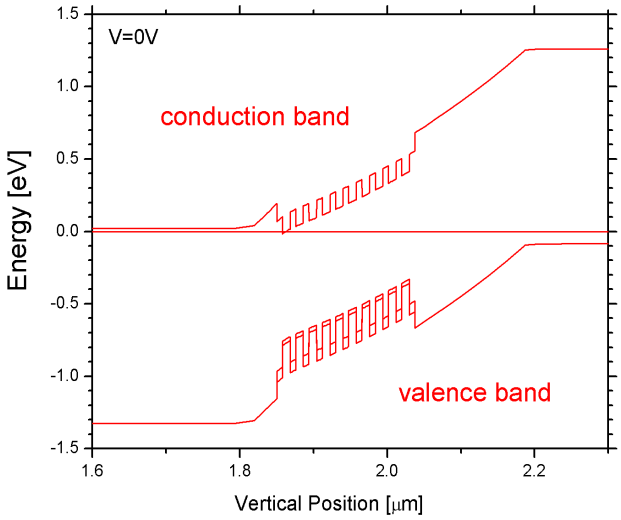

Figure 4. Energy band diagram of MQW active region with edges of heavy hole band, light hole band, and conduction band.

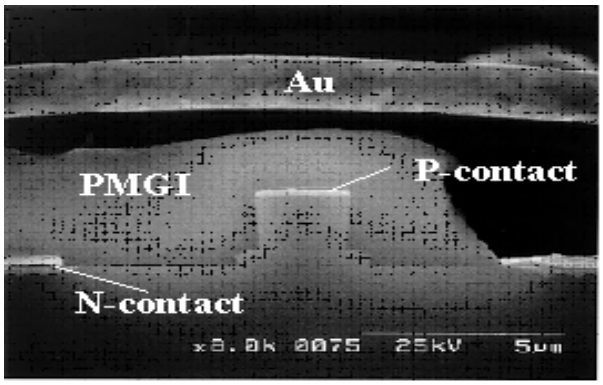

Figure 5. Facet view of a finished electroabsorption modulator.

The feed line is 500 μm long on each side of the optical waveguide. PMGI bridges are formed on both ends of the optical waveguide to connect grounds from different sides of the optical waveguide.

We have previously reported on the high modulation bandwidth of 25 GHz measured on our devices.[3] In this paper, we focus on the extinction efficiency. Transmission characteristics measured on recently fabricated devices are shown in Fig. 7 as function of reverse voltage for TM and TE mode. The most impressive feature of the transmission characteristics is the steep slope in the 0...2V range. The peak extinction efficiency is 35dB/V for the TM mode with a total modulation depth of 47dB. Consequently, the drive signal can be less than 1V for high bit rate modulation. At zero bias, the transmission loss is about -14 dB for the TE mode and -18 dB for the TM mode. This loss can be attributed to fiber coupling loss (about -6 dB), sidewall scattering loss, free carrier absorption, or residual quantum well absorption.

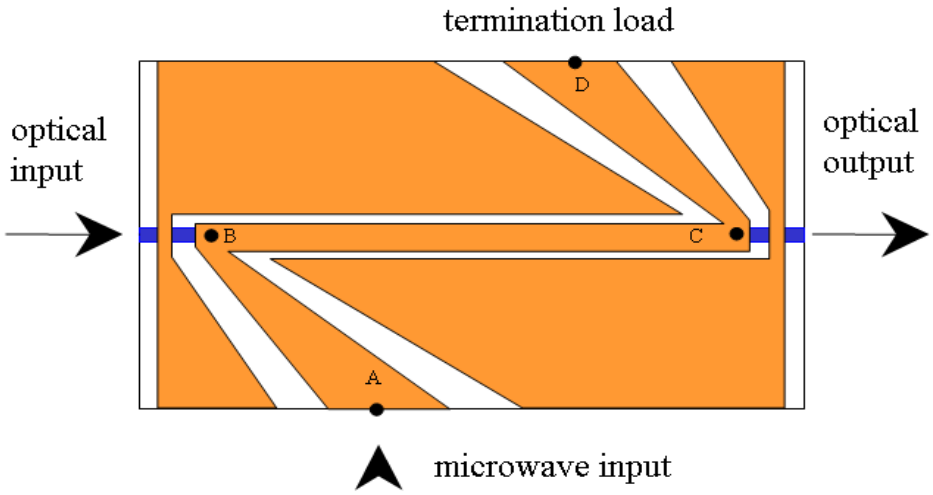

Figure 6. Co-planar waveguide design.

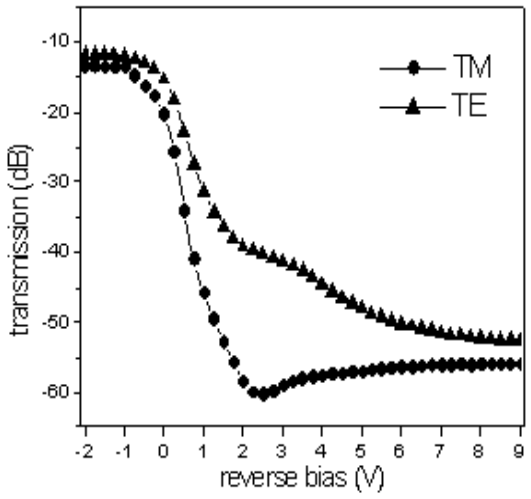

Figure 7. Transmission as function of reverse voltage measured at 1550 nm signal wavelength for TM and TE modes.

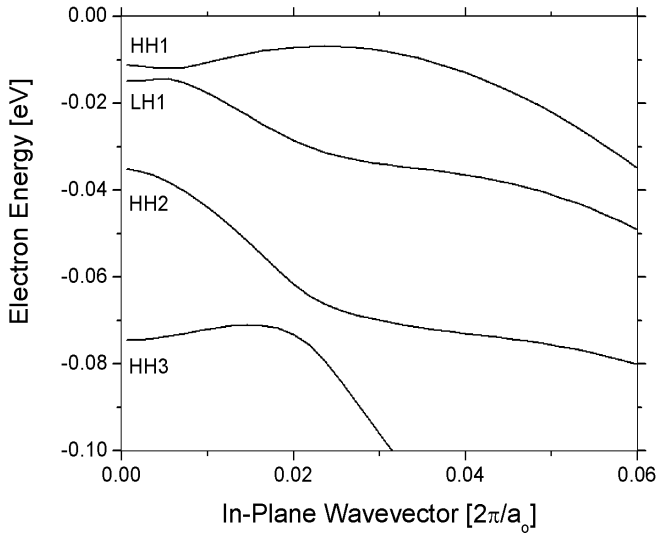

Figure 8. Valence subbands for polarization insensitive design (HH# - heavy hole subbands, LH# - light hole subbands).

3. SIMULATION AND ANALYSIS

Further performance optimization requires a detailed analysis of internal physical processes and their interaction. For this purpose, we employ a two-dimensional self-consistent EAM model to analyze and optimize our devices.[4] Comprehensive experimental results from Ref.[5] are used for model calibration and validation. The model self-consistently combines kp bandstructure and absorption calculations with a drift-diffusion model and optical waveguiding. The degeneration of heavy and light hole levels in our quantum wells is accompanied by an enhanced interaction of both particles. This interaction causes a substantial deformation of the valence subbands (valence band mixing). Fig. 8 shows the resulting non-parabolic shape of the valence bands.

The fundamental optical mode is shown in Fig. 9 for half the device cross section. The narrow ridge eliminates higher order modes and it gives a more circular mode profile for better coupling to optical fibers. The vertical refractive index profile is plotted in Fig. 10 together with the mode intensity. Stronger optical confinement is desired for low voltage operation, however, it causes higher fiber coupling losses. The optical model includes absorption losses by intraband transitions of free carriers and by intervalence band transitions. Both are roughly proportional to the carrier density and only relevant in p-doped regions. Figure 10 shows the resulting absorption profile. Due to the small overlap with the optical mode, the modal optical loss due to holes is only 1.5 cm^{-1}. Stronger optical losses are usually caused by photon scattering at the rough sidewalls of the etched waveguide, however, scattering losses are hard to calculate. The strongest contribution to the internal optical loss seems to result from the residual interband absorption at zero voltage.

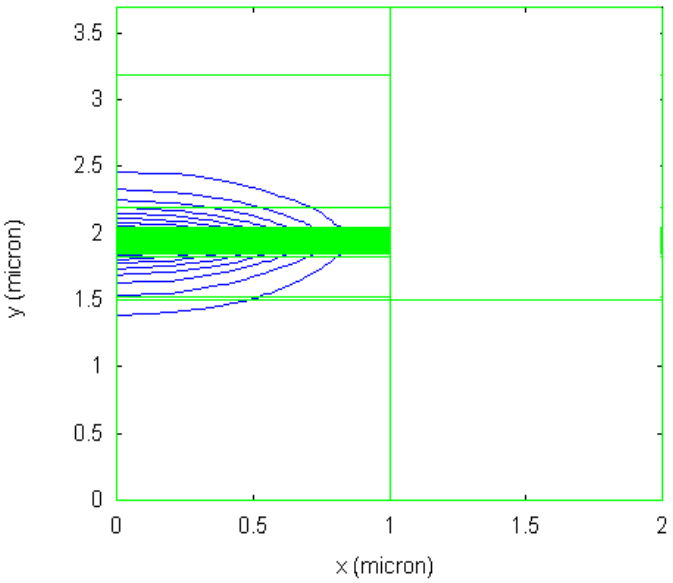

Figure 9. Half cross-section of the modulator waveguide with fundamental optical mode (the left border is the vertical symmetry plane of the device, the narrow lines indicate the MQW).

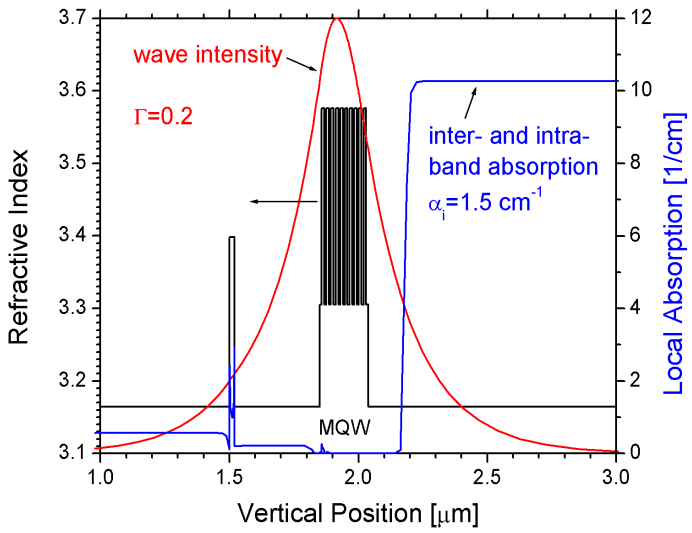

Figure 10. Vertical profile of refractive index, optical mode, and hole related absorption.

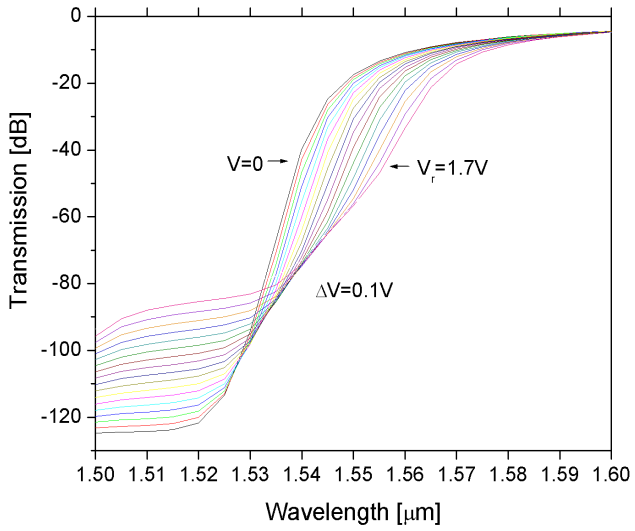

Figure 11. Optical transmission vs. wavelength with the reverse bias as parameter.

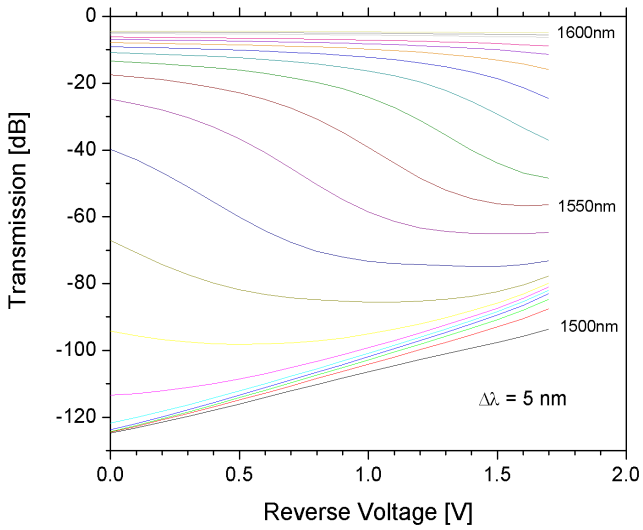

Figure 12. Optical transmission vs. reverse bias with the wavelength as parameter.

The optical transmission $T(\lambda, V)$ of the modulator is a function of the wavelength λ and of the applied reverse voltage V. The calculated transmission characteristics are shown in Fig. 11 as function of wavelength with the bias as parameter. As expected, with increasing reverse bias, the absorption edge moves towards longer wavelengths and the maximum absorption is reduced. In accordance to typical measurements, Fig. 12 displays the same transmission T as function of voltage with the wavelength as parameter. Minimum absorption occurs at the upper end of the spectrum (1600 nm) and maximum absorption at the lower end (1500 nm). At 1550nm, the transmission is reduced with higher reverse voltage, as seen in Fig. 11. For 1560 nm wavelength, the calculated transmission curves are compared to measurements from Ref.[5] showing

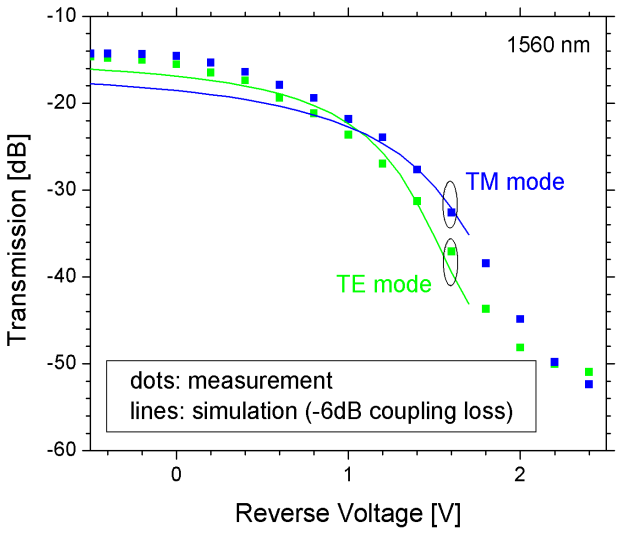

Figure 13. Comparison of measured and simulated transmission characteristics.

good agreement. The scattering time of 200 fs is used as fit parameter. However, due to numerical instabilities, transmission curves for more than 1.7 V reverse voltage could not be calculated. The device used in Fig. 7 has a slightly different active region design which leads to somewhat different transmission curves. More data on this new device need to be collected before better agreement can be achieved.

The steepest slope of $T(V)$ in Fig. 12 occurs at about 1V reverse voltage, which gives the highest extinction efficiency. However, practical applications also require high total light transmission. Therefore, we here use $T \times dT/dV$ as figure of merit which is plotted in Fig. 14 for three different wavelengths. The optimum voltage for maximum efficiency is slightly below 1V for 1550 nm wavelength. Fig. 14 emphazises the strong wavelength dependence of quantum-well EAM performance which was already indicated by previous figures.

Linearity is another main requirement in practical applications of EAMs. Ideally, both the second derivative d^2T/dV^2 and the third derivative d^3T/dV^3 of the transmission function $T(V)$ should be zero. However, this is hard to achieve and we are using the sum of both the derivatives as figure of merit which is plotted in Fig. 15. At 1550 nm wavelength, the optimum reverse bias for maximum linearity is close to 0.7 V since both the derivatives compensate each other at this voltage. The figure of merit shows a maximum at the voltage of highest efficiency (0.95 V). Thus, maximum efficiency and maximum linearity cannot be achieved simultaneously.

4. SUMMARY

High-performance multi-quantum well electroabsorption modulators are demonstrated. To the best of our knowledge, our peak extinction efficiency of 35 dB/V is the highest ever measured at 1550 nm wavelength. Based on two-dimensional simulations of carrier transport, optical absorption, and optical waveguiding, we have analyzed internal physics of our devices. The internal optical loss seems to be dominated by residual

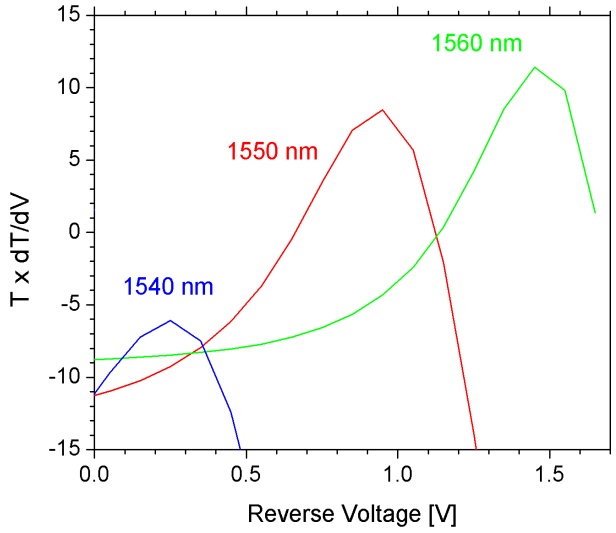

Figure 14. Transmission T [dB] times dT/dV [dB/V] as function of reverse bias for three different wavelengths.

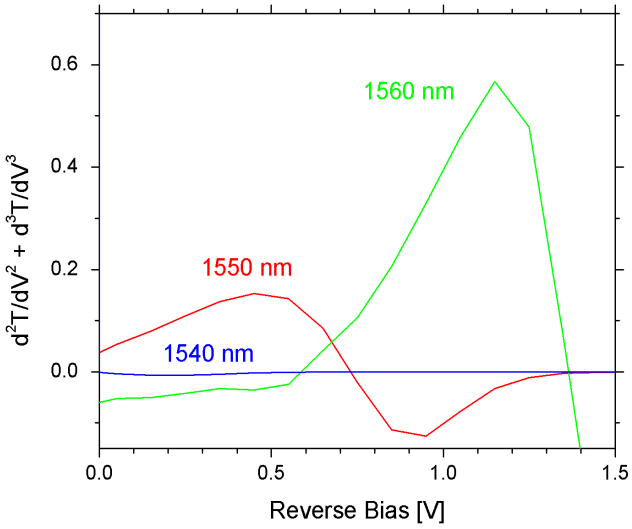

Figure 15. Sum of second and third derivative of the transmission function T(V) as function of reverse bias for three different wavelengths.

quantum well absorption. The calculated transmission characteristics exhibit a strong wavelength sensitivity. For transmission at 1550 nm, optimum reverse voltages are identified for maximum efficiency and maximum linearity, respectively.

REFERENCES

1. D. A. B. Miller, D. S. Chemla, T. C. Damen, A. C. Gossard, W. Wiegmann, T. H. Wood, and C. A. Burrus, "Electric field dependence of optical absorption near the band gap of quantum well structures," *Physical Review B* **32**, pp. 1043–1059, 1985.
2. C. Prott, *Optimization of the continuous wavelength tuning of laser diodes based on the quantum confined Stark effect*, Dissertation, University of Kassel, Germany, 2000.
3. S. Z. Zhang, Y.-J. Chiu, P. Abraham, and J. E. Bowers, "25-GHz polarization-insensitive electroabsorption modulators with traveling-wave electrodes," *IEEE Photonics Technology Letters* **11**, pp. 191–193, 1999.
4. LASTIP 6.1.1 by Crosslight Software, 2001.
5. S. Z. Zhang, *Traveling-wave electroabsorption modulators*, Ph.D. thesis, University of California at Santa Barbara, 1999.